Fall 2012

A study of wavelet-based noise reduction techniques in mammograms

Varun Shah

Department:

A STUDY OF WAVELET-BASED NOISE REDUCTION TECHNIQUES IN MAMMOGRAMS

by

VARUN SHAH

A THESIS

Presented to the Faculty of the Graduate School of the

MISSOURI UNIVERSITY OF SCIENCE AND TECHNOLOGY

In Partial Fulfillment of the Requirements for the Degree

MASTER OF SCIENCE IN ELECTRICAL ENGINEERING

2012

Approved by

Dr. Hyoung Koo Lee, Advisor
Dr. Randy H. Moss, Co-advisor
Dr. R. Joe Stanley

ABSTRACT

Breast cancer is one of the most common cancers and claims over one thousand lives every day. Breast cancer turns fatal only when diagnosed in late stages, but can be cured when diagnosed in its early stages. Over the last two decades, Digital Mammography has served the diagnosis of breast cancer. It is a very powerful aid for early detection of breast cancer. However, the images produced by mammography typically contain a great amount noise from the inherent characteristics of the imaging system and the radiation involved. Shot noise or quantum noise is the most significant noise which emerges as a result of uneven distribution of incident photons on the receptor. The X-ray dose given to patients must be minimized because of the risk of exposure. This noise present in mammograms manifests itself more when the dose of X-ray radiation is less and therefore needs to be treated before enhancing the mammogram for contrast and clarity. Several approaches have been taken to reduce the amount of noise in mammograms. This thesis presents a study of the wavelet-based techniques employed for noise reduction in mammograms.

ACKNOWLEDGEMENTS

I am greatly indebted to my advisor, Dr. Hyoung Koo Lee, for providing me with an opportunity to pursue this research. I sincerely thank him for the constant support, encouragement and guidance he provided that allowed me to complete this work. I am extremely grateful to him for sharing his expert knowledge and ideas and teaching me the basics of research. I am also thankful to him for supporting me financially.

I would like to thank Dr. Randy Moss for being my co-advisor and serving on my committee. I am very grateful to him for helping me with the formalities to do an out-of-department research. I would also like to thank Dr. Joe Stanley for serving on my committee and examining my thesis. He has been extremely supportive.

I would take this opportunity to thank my parents Vinod Shah and Jyoti Shah, and my brother Siddharth Shah for having faith in me and supporting me in all situations.

Lastly, I would like to thank all my friends in Rolla and back home who have always been understanding and helpful.

This thesis is dedicated to my advisor and my family.

TABLE OF CONTENTS

Page

LIST OF ILLUSTRATIONS

LIST OF TABLES

1. INTRODUCTION

1.1. MOTIVATION

Breast cancer or Malignant Breast Neoplasm is the most common type of cancer in women. It originates most commonly from the inner lining of ducts or the lobules that supply the ducts with milk. Worldwide, breast cancer comprises 22.9% of cancers in women and causes approximately 500,000 deaths every year. It can be treated depending on the size, stage, growth rate and other characteristics of the tumor; but a late diagnosis can prove to be fatal too. For this reason, it is best if the cancer is diagnosed in its early stages. There are several ways of examining breasts for early detection of breast cancer - Mammography, MRI (Magnetic Resonance Imaging), Clinical Breast Exam, Breast cancer screening etc. Figure 1.1 shows the mammogram of a woman diagnosed with breast cancer. The arrows in the figure point at micro-calcification.

Mammography is the use of low-energy X-rays to examine the human breast. It is used by the radiologists in the early detection of breast cancer through detection of micro-calcifications. All mammography systems have inherent noise which degrades the visual appearance of digital mammograms and gives the image a mottled, grainy, textured or snowy appearance thus making it difficult to detect micro-calcifications.

Several techniques have been proposed both in the spatial and frequency domain to reduce/remove the noise present in digital mammograms. Transformations/manipulations in the frequency domain using wavelet transforms have yielded very good digital images with reduced noise. Wavelet domain also has other added advantages which are discussed in the next chapter. This thesis presents a study of 5 different wavelet-based noise reduction techniques in Digital Mammograms.

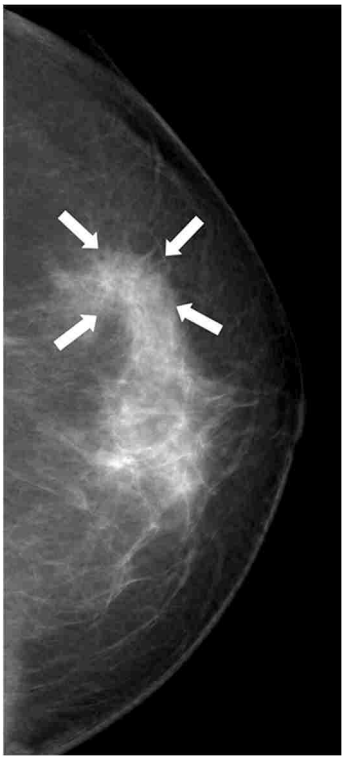

Figure 1.1 Mammogram of a woman diagnosed with breast cancer

1.2. DIGITAL MAMMOGRAPHY

Over the last decade, digital mammography has been increasingly replacing the conventional screen-film mammography because in a screen-film mammography system, the output is simply a film with an X-ray image of the breast. This film cannot be processed or manipulated for better visual appearance while a digital mammography system is known for the ease of manipulation to improve the visual quality of digital mammograms. Studies have demonstrated that a digital mammography system is at least as accurate as a conventional screen-film mammography system [1]. Figure 1.2 below demonstrates the difference in visual quality of a digital and screen-film mammogram.

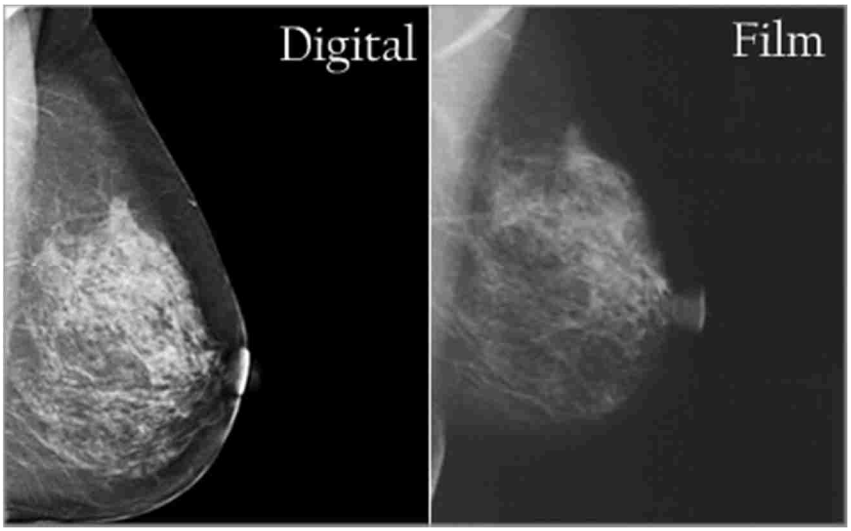

Figure 1.2 Digital mammogram (left) vs. Screen-film mammogram

The basic difference between screen-film mammography and digital mammography is the use of digital receptors in place of X-ray film in digital mammography systems. The digital receptors transduce incident X-rays into electrical signals which are conditioned and displayed as digital images on computer screens. In younger women, digital mammography presents significant improvements over the conventional screen-film mammography.

There are several advantages of using a digital mammography System [2]:

- ✓ Digital mammograms can be viewed in different orientations, magnifications and brightnesses to make them more discernible just by pixel manipulation.
- ✓ Digital mammograms are more storage friendly since they can be stored electronically. This enables ease of remote access and retrieval for distant consultation and diagnosis.
- ✓ Digital mammograms have also been found to give fewer false positives when compared with screen-film mammography.
- ✓ Studies show that digital mammography leads to a fewer number of recalls or repeat mammograms.

- ✓ Faster image acquisition (less than a minute as compared to several minutes in screen-film mammography) is achieved.
- ✓ Digital mammography has a short exam time, hence more number of mammograms can be generated in a given time.
- ✓ Lastly and most importantly, a digital mammography system gives a lesser dose (up to 50%) of X-ray radiation to the patient when compared with a screen-film mammography system. [2]

2. BACKGROUND

The three factors that constitute the quality of an image are noise, contrast and sharpness.

- ✓ **Noise** – is the unwanted variation in brightness of an image.
- ✓ **Contrast** – is the difference in luminance or pixel value (intensity) that makes an object discernible from its background or other objects.
- ✓ **Sharpness** – is the amount of details an image can convey

It is evident from the above definitions that an image with low noise and high contrast and sharpness is desired. Contrast and sharpness play very important roles in making the different anatomical parts in an X-ray or mammogram discernible. The digital radiography and mammography systems that are used today produce crude images with a very low contrast and sharpness. Thus, various digital image processing techniques are employed to improve contrast and sharpness of a digital image. But the underlying problem is that most of these image processing techniques tend to enhance the inherent noise present in the raw image. Therefore, it is necessary to free these images from noise and then process them for a better contrast and sharpness.

2.1. IMAGE NOISE

Noise means an unwanted sound. In the context of images, image noise also known as image mottle, is an unwanted variation of brightness or color information in a displayed image even when no image detail is present. This variation is usually random and has no particular pattern. This is especially significant when the images have a low contrast. It can be produced by the underlying circuit in the receptor or in the film grain or due to the characteristics of incident photons. This noise level can vary from almost imperceptible specks on a photograph clicked in good ambient light, to astronomical images which almost entirely consist of noise. It is from these

noisy images that we extract useful details/information about the subject of the image. Figure 2.1 below shows an example of clean image and a noisy version of it.

Figure 2.1 Original Lena image (left); noisy Lena image (right)

All medical images tend to contain some visual noise. Medical images generally refer to images from radiography systems, fluoroscopy systems, MRI (Magnetic Resonance Imaging) scanners, photo-acoustic systems, breast thermography systems, CT (Computed Tomography) systems or ultrasound imaging systems. Noise is more prevalent in certain types of imaging systems than others. The noise present in these images degrades the visual appearance of an image by making it grainy, thus hiding the actual features of the image. This effect is most evident and significant in low-contrast images when the images are very close to their visibility threshold. The visibility threshold for low-contrast objects is very noise dependent. When we reduce image noise, more of low-contrast objects within the body become visible.

2.2. TYPES OF NOISE IN RADIOGRAPY IMAGES

2.2.1. Quantum Noise. In an X-ray imaging system such as a digital mammography system, the X-ray photons impinge on digital image receptors. Nothing can cause them to be evenly distributed over the receiving surface. Thus, one area of the receptor might have more photons incident on its surface than another area even when both the areas are exposed to the same average X-ray intensity. The image noise produced by the random fashion in which the photons are distributed in an image is designated as quantum noise or shot noise or quantum mottle. It is determined by the variation in incident X-ray photon concentration.

From Figure 2.2 below, the most important characteristic of quantum noise is observed– it can be reduced by increasing the concentration of photons or exposure used to produce an image. The deviation described in the Figure 2.2 below follows a Poisson distribution. Mathematically speaking, quantum noise is inversely proportional to the square root of the exposure or concentration of photons [3].

There is a fundamental tradeoff between image noise and required exposure. A high patient exposure can be harmful but yield a good image quality. This image will have a higher magnitude of absolute noise but a very high visual quality since the magnitude of useful information is quite high. But this approach cannot be followed since this increases the risk of harming the patient and more specifically, the risk of breast cancer in case of digital mammography systems. So to keep a patient safe, the patient exposure can be reduced but at the expense of an increased quantum mottle. Thus the point of operation of most digital mammography procedures is a compromise between patient exposure and noise in the obtained image.

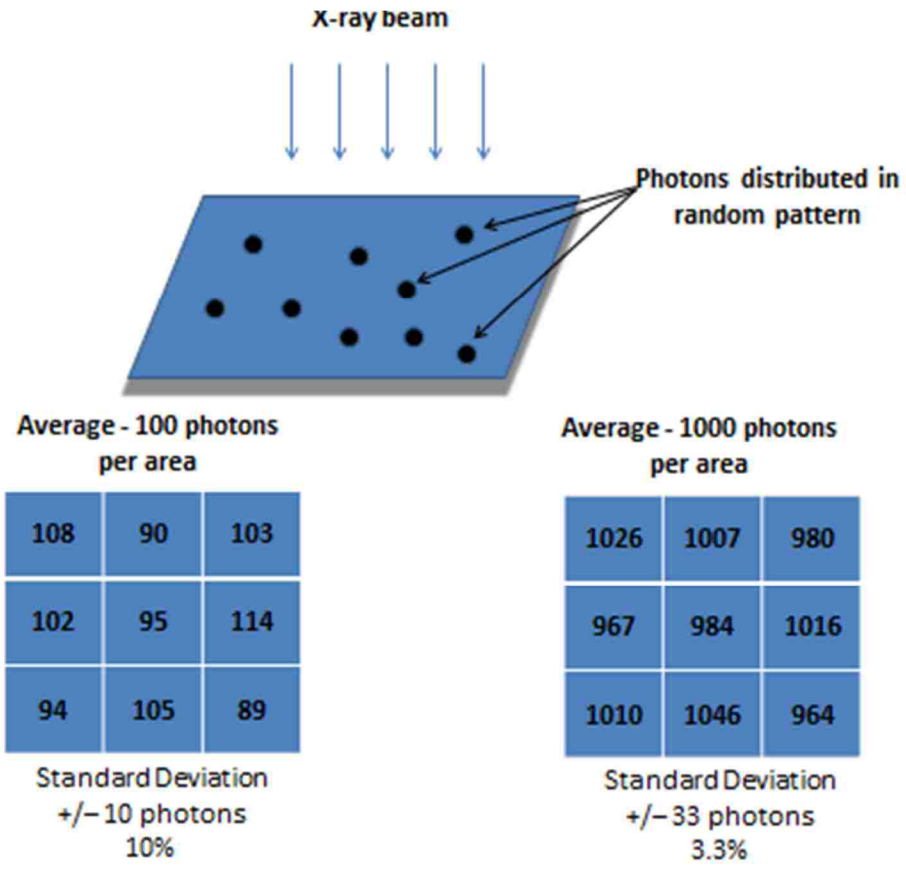

Figure 2.2 The concept of quantum noise

In different words, shot noise is the predominating unwanted factor in the brighter areas of an image where the intensity or pixel value is high. It has a root mean square value proportional to the square root of the image intensity. Also, the noises at different pixels are independent of each other or random. Shot noise is thus found to follow a Poisson distribution which is very close to Gaussian distribution [3].

The Poisson distribution expresses the probability of given events in a limited time or space given the average rate of occurrence of the events and the fact that they occur

independently of time or space of the last event [4]. This means that it predicts a degree of spread around a given average rate of occurrence. The variance of a Poisson distribution is equal to its mean.

For a given average rate or variance λ, the probability of occurrence of $X = k$ is given by [4]:

$$\Pr(X = k) = \frac{\lambda^k e^{-\lambda}}{k!}$$

To summarize, the characteristics of quantum noise are –

- ✓ It is the most significant contributor to noise in radiography or mammography images.
- ✓ There is always a tradeoff between the image noise and patient exposure to X-rays.
- ✓ The magnitude of quantum noise is higher in brighter areas of the image, i.e., the portions of the image with higher intensity.
- ✓ Quantum noise follows a Poisson distribution.

2.2.2. Grain and Structure Noise. For the case of screen-film mammography, the structure of the film, intensifying screens, intensifier tube screens or digital receptors can introduce noise into images. A film consists of several small silver halide crystals or grains. These grains become visible when an image on screen-film is optically enlarged or projected onto a screen. This film grain is a form of noise.

The image-intensifying screens and the screens of intensifier tubes are layers of very small crystals. This crystal structure presents a slight variation in light production from point to point in an image. This is designated as structure noise. This noise is usually insignificant in most radiographs.

2.2.3. Electronic Noise. Noise often gets introduced into a system from the leakage currents and any other random electrical currents produced by thermal activity in a device. These devices have a gain or amplification circuit for the amplification of weak signals. These circuits end up amplifying noise along with the signal thus making the noise very evident in an image.

Of all the noise sources discussed above, quantum mottle forms the most significant part of noise in any radiography image. Quantum mottle has noise intensity vs. frequency plot very close to an exponentially decreasing curve, i.e., it has a high intensity at lower frequencies and vice versa.

2.3. FACTORS AFFECTING NOISE

There are numerous factors which affect the different kinds of noise in radiography images described above –

- ✓ **Pixel size**- The larger a pixel is, the more photons are incident on it. This gives rise to a better Signal-to-Noise Ratio (abbreviated as SNR) for a particular exposure. Noise power is directly proportional to the area of the sensor while noise voltage is directly proportional to the square root of power (as expected) or area. If the dimensions of a sensor are increased to 2 times (300% increase in area), the SNR is also doubled.
- ✓ **Receptor technology** - The two major technologies employed are CCD (Charge Coupled Device) and CMOS (Complementary Metal Oxide Semiconductor). Until the 21st century, CMOS showed a highly degraded performance with abundant noise in the images produced. But today, CMOS gives results comparable to CCD [3]. CMOS is less expensive, easy to manufacture and maintain.

- ✓ **Exposure** - Long exposures with reduced dose produce way more noisy images than short exposures with reasonable dose. Exposure can be high either due to tube current which means greater concentration of photons or due to higher exposure time.

2.4. NOISE METRICS

Knowing the existence of noise isn't good enough if it cannot be measured in quantity or numbers. There needs to be a well-defined metric which can quantify the amount of noise present in an image. This would also enable a measure of the amount of noise reduced by various noise reduction techniques. Thus, different noise reduction techniques can be compared and used according to the application. There are several techniques used for noise reduction. Before looking at these universally used metrics, it is good to know some characteristics of noise measurements. Noise measurements should:

- ✓ Have a relation with the perceived appearance
- ✓ Be in reference with the original scene
- ✓ Be simple to interpret and compute
- ✓ Incorporate good details of the image while calculating to give an accurate understanding of performance of a sensor/camera

The most widely used noise metrics are:

2.4.1 SNR (Signal to Noise Ratio). It is often used as a measure of sensitivity of an imaging system. SNR has been defined as the ratio of average value of signal (μ_{sig}) to the standard deviation of background (σ_{bg}). When the background is black, a better definition is the ratio of average value of signal (μ_{sig}) to standard deviation of signal (σ_{sig}).

$$SNR = \frac{\mu_{sig}}{\sigma_{sig}}$$

2.4.2 CNR (Contrast to Noise Ratio). It is often used as a measure of quality of image. This metric is more useful when the ROI (Region Of Interest) in an image is degraded uniformly. Two different areas in ROI are subtracted to cancel out the uniform degradation [5].

$$CNR = \frac{|S_A - S_B|}{\sigma_0}$$

S_A and S_B are the intensities (pixel values) of two different areas A and B in ROI and σ_0 is the standard deviation of the pure image noise

2.4.3 PSNR (Peak Signal to Noise Ratio). It is an often-used a metric to quantify the noise present in an image with reference to the original known-to-be-good image. It is the ratio between maximum possible power of a signal and the power of noise present. Since this could be a very big value, it is often expressed in a logarithmic scale. It is conveniently defined using the Mean Squared Error (MSE) which is computed using two $p\ x\ q$ monochrome (mono color plane) images X and Y. One of the images X or Y is a noisy approximation of the other [6].

$$\text{MSE} = \frac{1}{p\ q}\sum_{i=0}^{p-1}\sum_{j=0}^{q-1}[X(i,j) - Y(i,j)]^2$$

$$PSNR = 10 \cdot \log_{10}\left(\frac{MAX_I^2}{MSE}\right)$$

where, MAX_I is defined as the maximum intensity (pixel value) of the known-to-be-good image.

2.5. ADDED NOISE QUANTITY

In this thesis, Gaussian noise and Poisson noise is added to clean Lena image to form noisy images which undergo several de-noising techniques. Gaussian noise is added with a mean of 0 and a variance of 0.01. Poisson noise is generated from the image itself. The noisy pixel is

generated from a Poisson distribution of mean equal to or proportional to the input pixel depending on the number of significant bits in the input pixel.

2.6. NOISE FILTERS

There are several techniques employed for the removal of noise in images. All techniques have some characteristic parameter which is sensitive to the noise intensities of a particular kind of noise. By employing these techniques, the noise levels in radiography images and mammograms are reduced, post which these images can be processed for contrast and sharpness enhancement without the risk of enhancing noise.

Any technique applied to the images for noise reduction broadly falls under either of the two domains:

1. Spatial Domain 2. Frequency Domain

2.6.1. Spatial Domain Techniques. An image is a 2-dimensional or 3-dimensional matrix of numbers when represented digitally or electronically. Each of these numbers, more technically called the gray levels or intensity values, corresponds to a particular shade of gray in a gray level image, a particular color in a 2-D color image or a shade of Red, Green or Blue in an RGB image. Each element of this matrix is called a pixel.

As is evident, the visual appearance of the image changes as we modify these pixels. If these pixels are modified in a particular fashion or obeying a particular equation or a set of equations, a uniform change in the image can be expected. This is known as point to point processing.

$$g(x, y) = T[f(x, y)]$$

Here $g(x,y)$ is the output image, $f(x,y)$ is the input image, T is a transfer function between $f(x,y)$ and $g(x,y)$.

At times, a small window (matrix) $h(x,y)$ is defined with some weights and is applied to the whole image. This window scans through the image and modifies the pixel of the image where the window is centered. This modification involves the neighboring pixels and every neighbor contributes according to a weight factor defined in the window. This is known as spatial filtering.

$$g(x,y) = f(x,y) * h(x,y)$$

Here $f(x,y)$ is the input image and $g(x,y)$ is the output image which is obtained by the spatial-domain convolution ($*$) of input image $f(x,y)$ and weight matrix $h(x,y)$.

2.6.1.1. Smoothing filters. A smoothing filter sets each pixel to the average value or a weighted average value of itself and its neighboring pixels. This basically smoothens or averages an image and sets every pixel much closer in intensity to its neighbors. Since, noise is essentially a random high magnitude variation in intensity, using a smoothing filter would degrade the noise to an intensity level close to its neighbors. This is essentially a linear technique because the whole image undergoes the same linear manipulation.

It can be seen from Figure 2.3 that with averaging, the amount of noise reduces but the edges are blurred. For this reason, averaging is not considered a good technique for noise reduction [7].

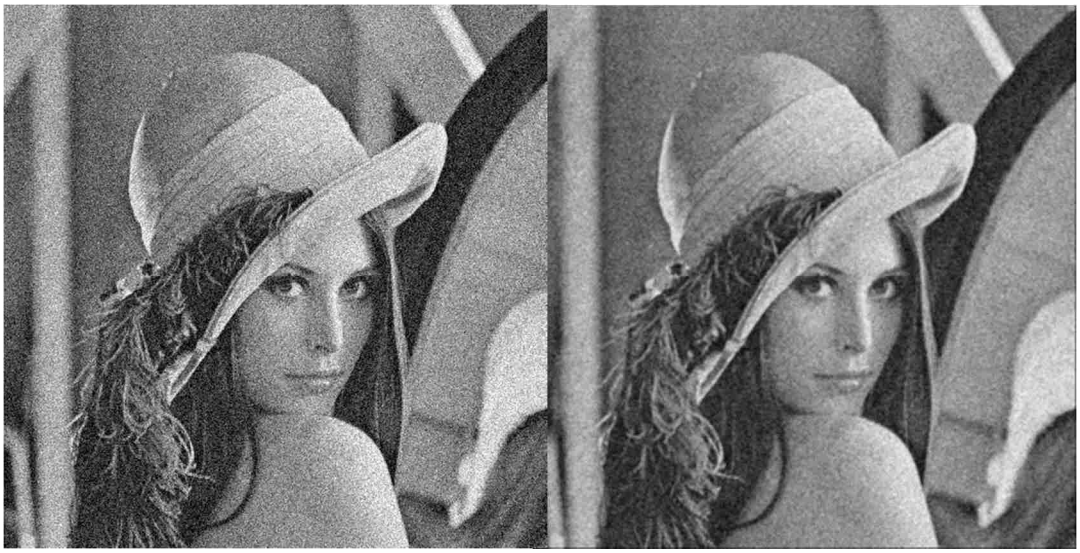

Figure 2.3 Lena image with Gaussian noise (left); averaged image (right)

2.6.1.2. Median filters. A median filter sets each pixel to the median of itself and its neighboring pixels. This filter modifies the noisy intensity values to a lower intensity value close to its neighbors and thus aims at lowering noise. This kind of filter is good at removing salt and pepper noise. This is a non-linear technique since the modification doesn't obey a linear equation or manipulation [7].

Figure 2.4 demonstrates the result of median filtering. Median filtering presents a significant reduction in noise while the edges are preserved better than by averaging.

Figure 2.4 Lena image with Gaussian noise (left); median filtered image (right)

2.6.1.3. Fuzzy-logic based techniques. Fuzzy means multiple-valued. In the context of image processing, fuzzy logic means there are multiple transfer functions between an input and output pixel. Every input pixel is evaluated for its membership in a given parameter space. There are rules for every different kind of membership which define the transfer function between the input and output pixel. In other words, there are different mappings between the input and output pixel based on membership. Such techniques are called adaptive. They adapt to the input to produce an output [8].

Fuzzy-logic based techniques work best in photographic images where the edges are long. In case of radiography images, especially mammograms, the edges are too small and very close to each other. This makes it difficult to design mappings which will preserve the edges and aid noise reduction. Thus, it is difficult to avoid producing artifacts when dealing with mammograms.

2.6.2. Frequency Domain Techniques. Image processing in the frequency domain involves 3 basic steps:

- ✓ Transforming an image into its frequency (Fourier) represntation
- ✓ Perform image processing by modifying the Fourier representation
- ✓ Computer inverse transform into spatial domain

When there exists a high-magnitude variation in intensity over a fixed spatial distance (measured in pixels), it corresponds to a high frequency. If an object being imaged is homogenous, i.e. if the variation in intensity is not too high, it corresponds to a low-frequency.

From the characteristics of noise as discussed earlier, noise is a high frequency component. Thus in order to eliminate/reduce noise in an image, the high frequency components need to be removed. As is obvious, the edges of an image also correspond to high frequency. This complicates the process of noise filtering as edges need to be preserved in order to maintain the quality of an image. Thus, a low-pass filter with some edge preserving mechanism is needed to remove noise while preserving edges.

2.7. WAVELET DOMAIN ANALYSIS

Wavelets are mathematical functions with Time-frequency representation (TFR). In this context, TFR refers to space-frequency representation. Unlike the spatial domain or frequency domain representation which only describes either the spatial or frequency distribution of intensities, a wavelet transform describes both spatial and frequency distribution of intensities at the same time. Wavelet transforms are multi-resolution decompositions that can be used to analyze signals and images. They describe a signal by the power at each scale and position.

2.7.1. Multi-scale Processing. With wavelets is achieved what is known as multi-scale processing. It is a very commonly used noise reduction technique. This approach was first introduced by Laine et al to digital mammography in 1994 [9]. A wavelet transform basically decomposes the input image into its high frequency and low frequency components. The low frequency coefficients usually carry the contrast information while the high frequency coefficients (horizontal details, vertical details and diagonal details) contain the edge information or detail information. [7] [10] [11]. As discussed earlier, the high frequency coefficients also contain noise. Therefore it is evident that for the reduction of noise, high frequency components must be modified. Once the coefficients are modified, the output image is reconstructed from the modified coefficient using the inverse wavelet transform.

2.7.2. Multi-resolution Analysis. An image is composed of connected regions of similar texture and intensity levels that combine to form objects. If objects are small in size, the analysis usually requires high resolution; on the other hand when they are large in size then coarse view suffices the requirement. If both the situations are present simultaneously like in mammograms, having several resolutions help in examining the image more efficiently. This is the motivation behind multi-resolution processing.

2.7.3. Wavelet Decomposition. Various filters could be used to decompose the image into high frequency and low frequency coefficients. A few examples are Daubechies, Coiflets, Symlets, Discrete Meyer, Bi-orthogonal and Reverse bi-orthogonal [7]. A wavelet decomposition decomposes an image into low frequency coefficients and high frequency coefficients. These components are half the dimension of the original image, i.e. if the image I has a size $(X \times Y)$, the size of the coefficients is $\left(\frac{X}{2} \times \frac{Y}{2}\right)$ [7]. This wavelet transform is termed as the first-order wavelet decomposition. If the low frequency component of size $\left(\frac{X}{2} \times \frac{Y}{2}\right)$ is further decomposed, it is known as the second-order decomposition. Now the sizes of coefficients is $\left(\frac{X}{4} \times \frac{Y}{4}\right)$. The decomposition

can go on further until dimension of coefficients is (1×1). Figure 2.5 below explains the concept of wavelet decomposition.

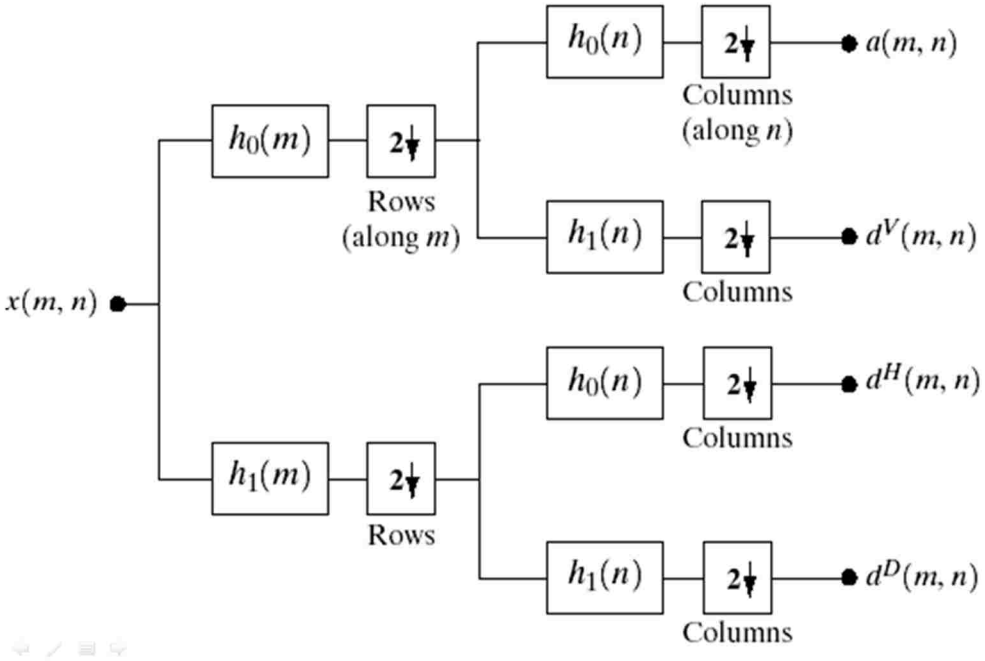

Figure 2.5 The concept of wavelet decomposition

Here, (↓) stands for down-sampling. Thus, an input image is down-sampled twice, once along each dimension to obtain the wavelet coefficients A (approximation), H (horizontal detail), V (vertical detail) and D (diagonal detail) coefficients.

Figure 2.6 below shows an image of size $(X \times Y)$. It was decomposed into four sets of coefficients LL_1, HL_1, LH_1 and HH_1. LL_1 is the set of low frequency components, also known as approximation coefficients. Since this $\left(\frac{X}{2} \times \frac{Y}{2}\right)$ matrix consists of low frequency components, it is a blurred version of the original image. It does not carry the detailed edge information of the

original image. HL_1, LH_1 and HH_1 are sets of high frequency coefficients. HL_1 is the set of horizontal detail coefficients; LH_1 is the set of vertical detail coefficients and HH_1 is the set of diagonal detail coefficients. As is obvious, to reduce noise, the high frequency coefficients HL_1, LH_1, and HH_1 need to be modified.

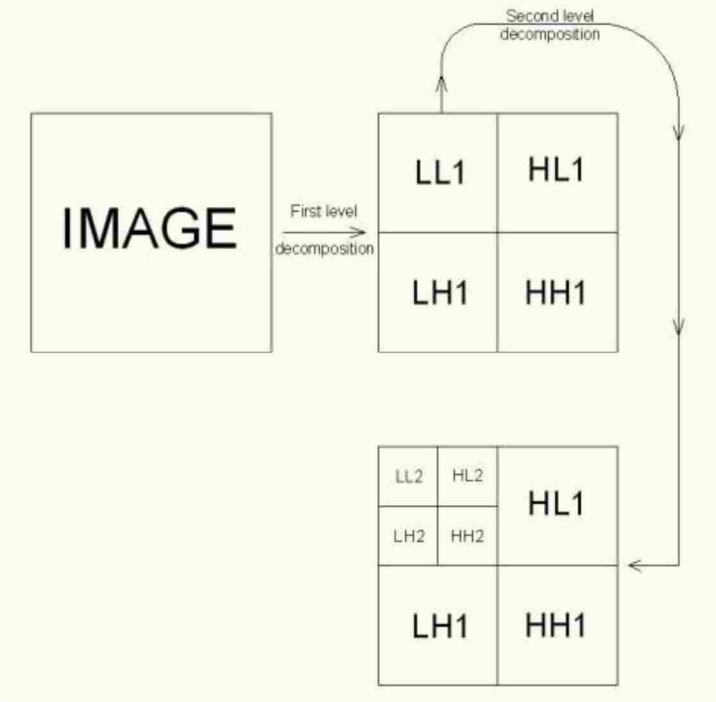

Figure 2.6 First and second level wavelet decomposition of an image

Similarly, the approximation low frequency coefficients LL_1 from the first level of decomposition can be treated as an image and further decomposed into its wavelet coefficients LL_2, HL_2, LH_2 and HH_2. These would be of size $\left(\frac{X}{4} \times \frac{Y}{4}\right)$. The blurred (version of original) image

LL_1 still has some edges visible along with other homogenous objects. The second level of decomposition separates the low and high frequency components leaving behind LL_2 which is a blurred version of LL_1. This process could keep continuing until the dimension of the set of coefficients is (1×1). Figure 2.7 below shows an image and its wavelet coefficients at levels 1 and 2.

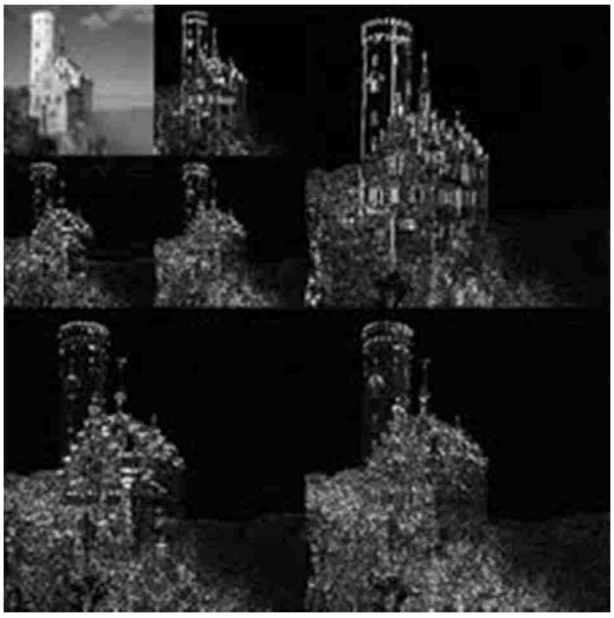

Figure 2.7 Wavelet decomposition at level 1 and 2

2.8. WAVELET BASED DE-NOISING

A de-noising algorithm based on wavelet transformation usually includes three steps:

1. Perform wavelet transformation of the image

2. Use different conditions of image and noise in the criterion space and remove noise from the image

3. Reconstruct the image by performing inverse wavelet transformation

De-noising in the wavelet domain can be generally divided into three kinds: the wavelet shrinkage method, the wavelet projection method and the wavelet correlation method. The wavelet shrinkage method is most commonly used because of the excellent noise reduction that has been achieved by its use [12]. The wavelet shrinkage method forms basis of study in this thesis.

Wavelet shrinkage method is a signal de-noising technique based on the idea of thresholding the wavelet coefficients. Wavelet coefficients having absolutely small value are considered to encode mostly noise and very fine details of the signal. The important information is encoded by the coefficients having a large absolute value. [13] [14]. Therefore removing small absolute value coefficients and then reconstructing the signal should produce signal with lesser amount of noise. The wavelet shrinkage approach can be summarized as follows:

- ✓ Apply the wavelet transform to the signal
- ✓ Estimate the threshold value
- ✓ Remove (zero-out) the coefficients that are smaller than the threshold
- ✓ Reconstruct the signal by applying the inverse transform

A very big challenge in wavelet shrinkage approach is finding an appropriate threshold value. The following section describes five different techniques used for finding a threshold value and applying the wavelet shrinkage method.

3. TECHNIQUES

3.1. TECHNIQUE 1 – DAUBECHIES COMPLEX WAVELET BASED SHRINKAGE

3.1.1. Principle. The fundamental equation guiding multi-resolution theory is the following scaling equation [15]:

$$\Phi(t) = 2\sum_{n} a_n \Phi(2t - n)$$

Where a_n's are coefficients and $\sum a_n = 1$.

Daubechies assumed the coefficients (a_n) to be real-valued. The symmetric Dabuechies complex wavelet transform is advantageous in that it has a good reconstruction property. The symmetric behavior enables easy handling of edge points during reconstruction.

3.1.2. Algorithm. The symmetric Daubechies complex wavelet transform of the image is computed. Then a decomposition level-dependent threshold is calculated as follows [16]:

$$T_j = \frac{1}{2^{j-1}}\left(\frac{\sigma}{\mu}\right)M$$

Where j is the resolution level, σ is the standard deviation of wavelet coefficients, μ is the mean of the absolute value of the wavelet coefficients and M is the median of the absolute value of coefficients at the j_{Th} level for a particular sub-band.

After calculating the threshold, a thresholding function is required to perform thresholding. Usually a hard or a soft thresholding function is used. But here, the following thresholding function is used:

$$\widehat{w} = \begin{cases} 0 & , \quad |w| < T \\ \left(1 - \frac{T^2}{w^2}\right), & |w| \geq T \end{cases}$$

Here T is the threshold, w is the wavelet coefficient and $\hat{w}$ is the thresholded wavelet coefficient. This thresholding is performed for all the horizontal, vertical and diagonal wavelet coefficients.

3.1.3. Results. Figure 3.1 below shows the de-noising technique applied to a mammogram.

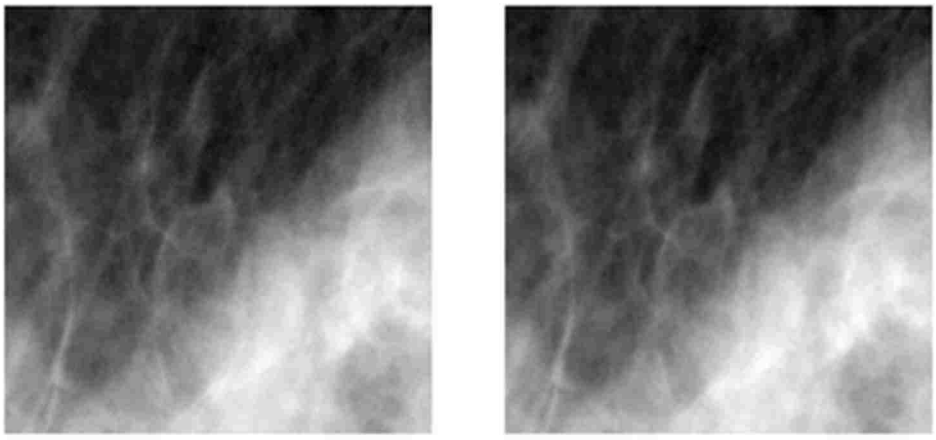

Figure 3.1 Original mammogram (512 x 512) (left); mammogram de-noised by Daubechies complex wavelet (right)

3.1.4. Discussion and Analysis. The image on the left in Figure 3.1 is de-noised with the technique discussed above. There is a slight reduction in noise as it can be seen visually. For the sake of quantifying the reduction in noise, the technique was applied to a Lena image with added Gaussian and Poisson noise. As discussed earlier, shot noise, which is the most dominant

noise in radiography images, is most accurately modeled as Poisson noise or approximately as Gaussian noise.

Figure 3.2 below shows the best achieved results of the technique applied to the Lena image. In the best results obtained, the PSNR of the de-noised image is about 5.5dB higher when the input was the Lena image with added Gaussian noise while the PSNR is about 2.2dB higher when the input was the Lena image with added Poisson noise.

Figure 3.2 Daubechies complex wavelet - Lena image with Gaussian noise (top-left); de-noised version of Lena image with Gaussian noise (top-right); Lena image with Poisson noise (bottom-left); de-noised version of Lena image with Poisson noise (bottom-right)

It is clear from Table 3.1 that, for decomposition levels of 3 and higher for Gaussian & 2 and higher for Poisson, the image started to degrade in terms of PSNR. It was observed that the images started to blur and develop artifacts which kept increasing in size with every level of decomposition. Therefore, a de-blurring technique has to be employed to obtain better results.

Table 3.1 Comparing PSNR by applying Daubechies complex wavelet at different decomposition levels

	Lena with Gaussian	Difference in PSNR	Lena with Poisson	Difference in PSNR
Noisy	19.7241	0	26.8579	0
Level 1	24.6879	4.9638	29.0186	2.1607
Level 2	25.4738	5.7497	26.4027	-0.4552
Level 3	23.2080	3.4839	23.3428	-3.5151
Level 4	20.6313	0.9072	20.6549	-6.203
Level 5	18.6091	-1.115	18.6164	-8.2415

3.2. TECHNIQUE 2 – FEATURE-BASED ADAPTIVE WAVELET SHRINKAGE FOR IMAGE DE-NOISING

3.2.1. Principle. This wavelet shrinkage approach applies the wavelet shrinkage function by adapting the features in an image [17]. Experiments performed on images have shown that a wavelet shrinkage method which incorporates energies of neighboring pixels improves the performance of the de-noising algorithm.

Assume a real image *f* and an observed image *g* which is corrupted by AWGN (Additive White Gaussian Noise) *n*:

$$g = f + n$$

After a wavelet transform,

$$W_g = W_f + W_n$$

The wavelet transform performs some degree of de-correlation thus implying that the wavelet coefficients corresponding to a high variation in intensity (say an edge) are clustered together and replicated across the different resolutions and sub-bands of a wavelet tree. The edges in an image are expressed by wavelet coefficients which are large in magnitude at the corresponding locations. Therefore by evaluating the energy in a localized area or window, the information about edges can be decoded. Homogenous objects are represented by coefficients smaller in magnitude and therefore contain lesser energy.

3.2.2. Algorithm. An (*RxR*) window is considered. The energy of wavelet coefficients is calculated in that window as follows [17]:

$$S_{x,y}^2 = \frac{1}{R^2} \sum_{m=1}^{R} \sum_{n=1}^{R} w_{m,n}^2$$

where *m,n* span the whole window of size (*RxR*), *w* is the wavelet coefficient and *x,y* span the entire set of high frequency coefficients.

$$\widehat{w_{x,y}} = \begin{cases} 0 & , \quad S_{x,y}^2 < \beta \cdot \lambda^2 \\ w_{x,y}\left(1 - \alpha * \frac{\lambda^2}{S_{x,y}^2}\right), & S_{x,y}^2 \geq \beta \cdot \lambda^2 \end{cases}$$

Where $\lambda^2 = (4\sigma^2 logR)$, $w_{x,y}$ is the center pixel in the window and $\widehat{w}_{x,y}$ is the output coefficient.

From experiments, the optimal values for α and β are found to be 0.1 and 0.3 respectively.

3.2.3. Results. Figure 3.3 below shows the de-noising technique applied to a mammogram.

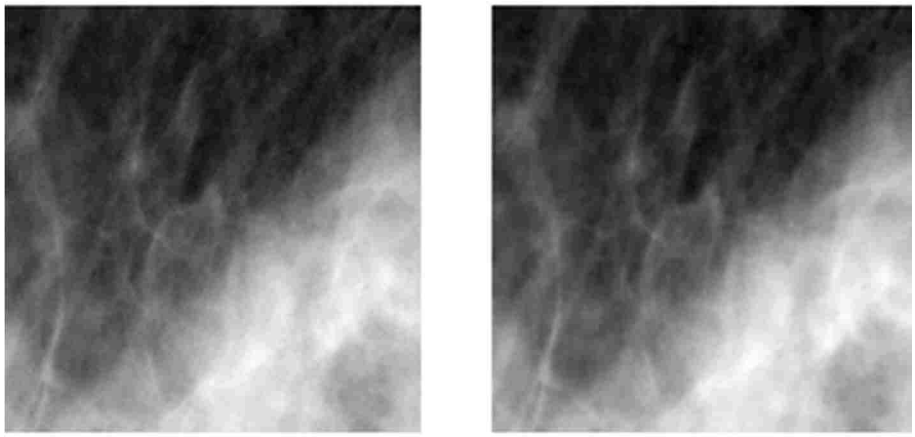

Figure 3.3 Original mammogram (512 x 512) (left); mammogram de-noised by feature-based wavelet (right)

3.2.4. Discussion and Analysis. The image on the left in Figure 3.3 is the original mammogram which is de-noised using the feature-based adaptive wavelet shrinkage discussed above. To quantitatively describe the performance of the technique, the same approach is applied to a Lena image with added Gaussian and Poisson noise. The windows used were (5x5) and

(7x7). The smaller window yielded better results which are shown in Figure 3.4. The PSNR of the noisy Lena image with Gaussian noise is found to be 19.8dB and that of the de-noised image to be 27.3dB. A significant decrease in noise is also observed in Lena image with added Poisson noise.

Figure 3.4 Feature-based wavelet - Lena image with Gaussian noise (top-left); de-noised version of Lena image with Gaussian noise (top-right); Lena image with Poisson noise (bottom-left); de-noised version of Lena image with Poisson noise (bottom-right)

From Table 3.2 below, the technique performs better with a window of size (5x5) than with a window of size (7x7). The PSNR is also found to increase until a decomposition level of 3 after which the PSNR starts to decrease.

Table 3.2 Comparing PSNR by applying feature-based wavelet at different decomposition levels

	Lena with Gaussian(5x5)	Difference in PSNR	Lena with Poisson(5x5)	Difference in PSNR
Noisy	19.8011	0	26.8444	0
Level 1	24.1663	4.3652	28.7212	1.8768
Level 2	26.5639	6.7268	29.1763	2.3319
Level 3	27.3123	7.5112	30.7961	3.9517
Level 4	26.8083	7.0072	28.6834	1.839
Level 5	24.2180	4.4169	27.9837	1.1393

	Lena with Gaussian(7x7)	Difference in PSNR	Lena with Poisson(7x7)	Difference in PSNR
Noisy	19.7201	0	26.7955	0
Level 1	23.5232	3.8031	27.9541	1.1586
Level 2	25.3589	5.6388	28.6215	1.862
Level 3	26.1086	6.3885	29.6548	2.8593
Level 4	25.8134	6.0933	27.2587	0.4632
Level 5	23.9458	4.2257	26.1395	-0.656

3.3. TECHNIQUE 3 – WAVELET SHRINKAGE USING STANDARD DEVIATION ESTIMATION

3.3.1.Principle. The image under study can be expressed mathematically as

$$f(x,y) = s(x,y) + n(x,y)$$

where $f(x,y)$ is the image signal, $s(x,y)$ is the target signal and $n(x,y)$ is the Gauss noise and obeys independent and identical distribution $N(0,\sigma^2)$, σ is the standard deviation of noise $n(x,y)$.

As discussed earlier, the wavelet de-noising process is carried out in the detail coefficients. A wavelet shrinkage method is used to process the high frequency component. A very common thresholding process known as soft-thresolding is used [18].

$$\widehat{w} = \begin{cases} 0 & , \quad |w| < T \\ sgn(w)(|w| - T), & |w| \geq T \end{cases}$$

Where w is the wavelet transformation coefficient, $\widehat{w}$ is the thresholded coefficient and T is the threshold.

3.3.2. Algorithm. The value of the threshold T is related to σ, the noise standard deviation. The value of the global threshold T is $\sigma\sqrt{2\ln N}$ where N is the length of the signal; the partial threshold value T is $\sigma\sqrt{2\ln N}\,/\ln(j+1)$ where j is the decomposition level number. In practical applications, σ is usually unknown. Therefore σ should be estimated for de-noising.

One way to estimate the noise standard deviation is to suppress the image structure using a Laplace template. The remaining part of the image is noise. The equations below are the Laplace operator and its discrete form respectively.

$$\nabla^2 f = \frac{\partial^2 f}{\partial x^2} + \frac{\partial^2 f}{\partial y^2}$$

$$\nabla^2 f = f(x+1,y) + f(x-1,y) + f(x,y+1) + f(x,y-1) - 4f(x,y)$$

From the discrete form, the approximation of two Laplace templates can be obtained:

$$L_1 = \begin{matrix} 0 & 1 & 0 \\ 1 & -4 & 1, \\ 0 & 1 & 0 \end{matrix} \qquad L_2 = \frac{1}{2}\begin{matrix} 1 & 0 & 1 \\ 0 & -4 & 0 \\ 1 & 0 & 1 \end{matrix}$$

By using the difference between the above two templates to suppress the image, noise can be estimated [19]. The noise estimation template *M* is,

$$M = 2(L_2 - L_1) = \begin{matrix} 1 & -2 & 1 \\ -2 & 4 & -2 \\ 1 & -2 & 1 \end{matrix}$$

Here the average value of *M* is zero. If the standard deviation of each element is σ_n^2, the variance of *M* is $36\sigma_n^2$. Computing the variance of output of the *M* operator applied to the image will give an estimate of $36\sigma_n^2$ at each pixel, which can be averaged over the image or local neighborhoods to give an estimate of the noise variance σ_n^2. Therefore the variance of noise in the image can be computed as [20]:

$$\sigma_n^2 = \frac{1}{36(W-2)(H-2)} \sum_{image} [f(x,y) * M]^2$$

where *W* and *H* are the width and height of the image *f(x,y)* respectively, * represents spatial-domain convolution.

If *n(x, y)* obeys the independent and identical distribution $N(0,\sigma^2)$, the calculation above can be simplified as following [19]:

$$\sigma_n = \sqrt{\frac{\pi}{2}} \frac{1}{6(W-2)(H-2)} \sum_{image} |f(x,y) * M|$$

3.3.3. Results. Figure 3.5 below shows the de-noising technique applied to a mammogram.

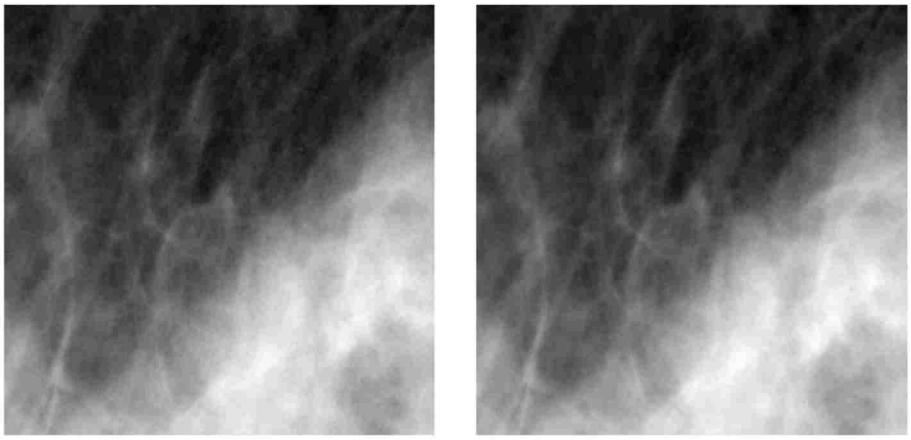

Figure 3.5 Original mammogram (512 x 512) (left); mammogram de-noised by standard deviation estimation (right)

3.3.4. Discussion and Analysis. The image on the left in Figure 3.5 is de-noised with the technique described above with a decomposition level of 1. For quantitatively expressing the amount of noise reduced, a cleaner image (or original image) of the input image is required as a reference to measure the PSNR (Peak Signal-to-Noise Ratio). Therefore, the same technique is performed on Lena image of the same size after adding Gaussian noise and Poisson noise as seen in Figure 3.6. The figure shows the best results obtained.

Figure 3.6 Standard deviation estimation - Lena image with Gaussian noise (top-left); de-noised version of Lena image with Gaussian noise (top-right); Lena image with Poisson noise (bottom-left); de-noised version of Lena image with Poisson noise (bottom-right)

As can be seen both visually and quantitatively, there is a good amount of reduction in noise after applying the technique. The Lena image with Gaussian noise has a PSNR of 19.7074, while the technique brings about close to 7dB of rise in PSNR. The Lena image with Poisson noise has a PSNR of about 26.8461. The technique brings the PSNR to 29.7804. From Table 3.3, it is observed that the PSNR increases up to a decomposition level of 2 for Gaussian & a decomposition level of 1 for Poisson and then starts to decrease. Therefore, this technique works best at a decomposition level of 2.

Table 3.3 Comparing PSNR by applying standard deviation estimation at different decomposition levels

	Lena with Gaussian	Difference in PSNR	Lena with Poisson	Difference in PSNR
Noisy	19.7074	0	26.8461	0
Level 1	24.7213	5.0139	29.7804	2.9343
Level 2	26.5118	6.8044	29.5744	2.7283
Level 3	26.1976	6.4902	29.0095	2.1634
Level 4	25.7697	6.0623	28.7198	1.8737
Level 5	25.5680	5.8606	28.6171	1.771

3.4. TECHNIQUE 4 – BAYESSHRINK METHOD

3.4.1. Principle. The threshold for wavelet shrinkage is derived in a Bayesian framework. The proposed threshold has a closed form and adapts to each sub-band (set of coefficients). This method outperforms Donoho and Johnstone's SureShrink method [21] which was a seminal work on image de-noising via wavelet shrinkage back in the early 90's. Wavelet shrinkage methods have shown to have better rates of convergence than linear methods of approximating functions in Besov spaces [13] [14].

Technique 3 described above is known to produce overly smooth images since the global threshold is $\sigma\sqrt{2\ln N}$. Here N (the number of samples) is large ($>10^5$) since the images being considered are of size *(512 x 512)*. The formulation of this technique is grounded on the empirical observation that the wavelet coefficients in the sub-band of an image can be adequately summarized by a Generalized Gaussian Distribution (GGD). From this observation, it follows

that the average MSE (Mean Squared Error) in a sub-band can be approximated by the corresponding Bayesian squared error. The thresholding process used is soft-thresolding:

$$\widehat{w} = \begin{cases} 0 & , \quad |w| < T \\ sgn(w)(|w| - T), & |w| \geq T \end{cases}$$

Where w is the wavelet transformation coefficient, $\widehat{w}$ is the thresholded coefficient and T is the threshold.

3.4.2 Algorithm. The noise variance σ^2 needs to be estimated first. In some situations, it may be possible to measure σ^2 based on information other than the corrupted image. But otherwise, it is estimated from the band HH_1 (which is the set of diagonal coefficients) by the Robust Median Estimator [18].

$$\sigma = \frac{Median(|Y_{ij}|)}{0.6745}, \qquad Y_{ij} \in subband\ HH_1$$

$$\sigma_Y^2 = \sigma_X^2 + \sigma^2$$

$$\text{(or)} \quad \sigma_x = \begin{cases} 0 & , \quad \sigma_Y^2 < \sigma^2 \\ \sqrt{\sigma_Y^2 - \sigma^2}, & \sigma_Y^2 \geq \sigma^2 \end{cases}$$

$$\text{(or)} \quad \sigma_X = \sqrt{\max(\sigma_Y^2 - \sigma^2, 0)}$$

where σ_Y^2 is the variance of Y. Since Y is modeled as zero-mean, σ_Y^2 can be found empirically by:

$$\sigma_Y^2 = \frac{1}{n^2} \sum_{i,j=1}^{n} {Y_{ij}}^2$$

where *(n x n)* is the size of the subband under consideration.

Thus threshold T_B is given by:

$$T_B = \frac{\sigma^2}{\sigma_X}$$

In the case of $\sigma_Y^2 < \sigma^2$, σ_X is taken to be *0*. That is T_B is ∞, or, in practice, $T_B = \max(|X_{i,j}|)$, and all coefficients are set to zero where $X_{i,j}$ is the entire matrix of wavelet coefficients.

3.4.3. Results. Figure 3.7 below shows the de-noising technique applied to a mammogram.

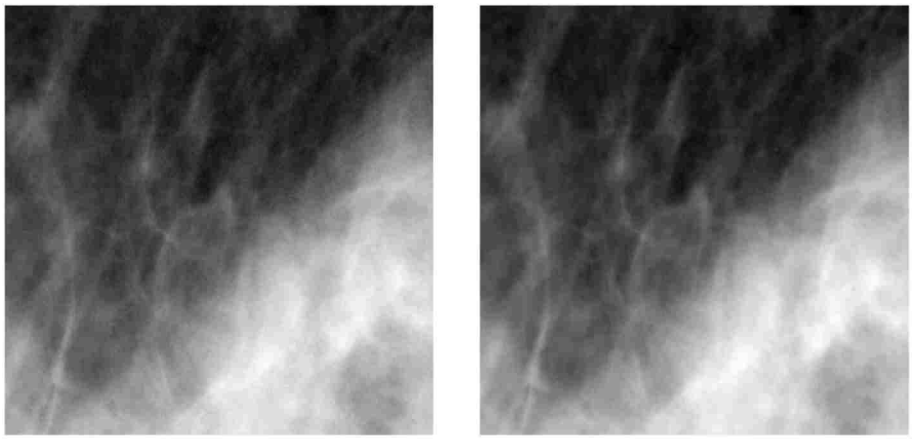

Figure 3.7 Original mammogram (512 x 512) (left); mammogram de-noised by BayesShrink (right)

3.4.4 Discussion and Analysis. The image on the left in Figure 3.7 is de-noised with the BayesShrink method and the de-noised image is presented on the right. To describe the effectiveness of the method quantitatively, BayesShrink method is applied to the Lena image with added Gaussian Noise and Poisson Noise as shown in Figure 3.8 below.

Figure 3.8 BayesShrink - Lena image with Gaussian noise (top-left); de-noised version of Lena image with Gaussian noise (top-right); Lena image with Poisson noise (bottom-left); de-noised version of Lena image with Poisson noise (bottom-right)

It is evident from Table 3.4 below that PSNR gets better with increasing levels of decomposition. At a decomposition level of 5, the BayesShrink method on the Lena image with added Gaussian noise shows a PSNR of 27.4814 which is almost 8dB higher than the noisy image. At the same decomposition level, the method on Lena image with added Poisson noise yields an image with PSNR of 31.1979 which is approximately 4.5dB higher than the noisy image. For these images, this is about the best that this method can produce. At decomposition

levels of 5, the reduction in noise starts to saturate. This can be seen clearly in the difference in PSNR values at levels 4 and 5.

Table 3.4 Comparing PSNR by applying BayesShrink at different decomposition levels

	Lena with Gaussian	Difference in PSNR	Lena with Poisson	Difference in PSNR
Noisy	19.6992	0	26.8542	0
Level 1	24.7177	5.0185	30.2943	3.4401
Level 2	27.0185	7.3193	31.1054	4.2512
Level 3	27.4422	7.743	31.1927	4.3385
Level 4	27.4786	7.7794	31.1977	4.3435
Level 5	27.4814	7.7822	31.1979	4.3487

3.5. TECHNIQUE 5 – MODIFIED BAYESSHRINK AND USE OF DAMF

3.5.1. Principle. When a signal is encompassed by additive Gaussian noise, its estimation is done by finding a wavelet basis that concentrates signal energy over few coefficients and by thresholding the noisy coefficients. However, it is found that, in many practical problems such as medical X-ray images, the recorded data are not modeled by Gaussian noise but as the realization of the Poisson process [22]. This method is an improvement over the BayesShrink approach [18]. To remove the large amplitude noise, a new type of filter called the Directional Adaptive Median Filter (DAMF) is used.

The thresholding process used is soft-thresolding as hard thresholding produces artifacts.

$$\widehat{w} = \begin{cases} 0 & , \quad |w| < T \\ sgn(w)(|w| - T), & |w| \geq T \end{cases}$$

where w is the wavelet transformation coefficient, $\widehat{w}$ is the thresholded coefficient and T is the threshold.

3.5.2 Algorithm. In the case of Poisson noise, where the noise variance is proportional to the image intensities, the BayesShrink approach has a disadvantage. It is only effective for small magnitude noise coefficients. Therefore a slightly modified approach is taken.

The variance of a Poisson random variable is equal to its mean. Thus, the variability of noise is proportional to intensity and, therefore image dependent. The noise power differs between wavelet coefficients according to the image pixel under the support of the associated wavelet basis function. This spatial variation of the noise needs to be accounted for in the filter design. Thus the algorithm of IBS and DAMF is proposed and applied in a sequence as shown in Figure 3.9.

3.5.2.1 IBS. It is found from experiments that wavelet coefficients of an X-ray image are smaller than a regular photographic image. This means the thresholds obtained by the BayesShrink method are not quite suitable for X-ray images. Therefore threshold is calculated by [22]:

$$T_B = \alpha \frac{\sigma^2}{\sigma_X}$$

Here α changes with the size of sub-band under consideration and the decomposition level. σ and σ_X are calculated the same way as in the BayesShrink method discussed above.

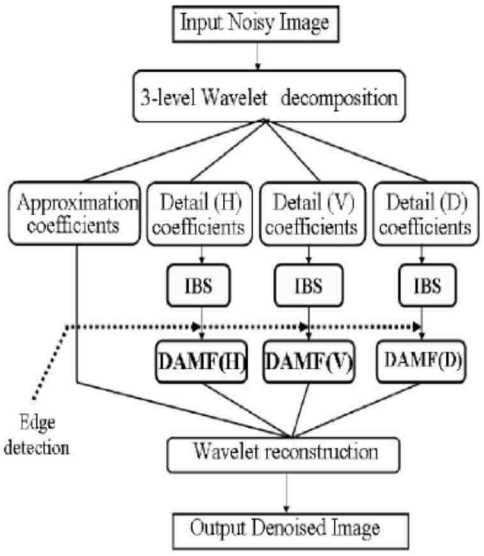

Figure 3.9 Algorithm of IBS and DAMF [22]

$$\alpha = \sqrt{\frac{\log(n^2)}{2xj}}$$

where n^2 is the size of sub-band under consideration and j is the decomposition level.

3.5.2.2 Edge detection in wavelet domain. To perform edge detection, it is assumed that when the absolute value of a wavelet coefficient is large, it is an edge. The algorithm is as follows:

i. The absolute values of thresholded coefficients are sorted from high to low. $W = \{w_1, \dots, w_i, \dots, w_N\}$.

ii. The sum of sorted coefficients SUM_n and SUM_N are calculated.

$$SUM_n = \sum_{i=1}^{n} abs(w_i)^2$$

$$SUM_N = \sum_{i=1}^{N} abs(w_i)^2$$

iii. Thresholding value in the sub-band is selected.

$$r = \frac{SUM_n}{SUM_N}$$

Where $r>v$ is the specific edge preservation percentage. In this study, $v=0.9$ has been used. w_n is the threshold of the edge detector.

iv. Edges are detected by the following criterion:

If $abs(w_i)^2 > abs(w_n)^2$, w_i is regarded as an edge, else w_i is regarded as noise and is processed by DAMF(discussed below).

3.5.2.3 Directional adaptive median filter (DAMF). DAMF is designed for three directions, each for the corresponding sub-band. Figure 3.10 below shows the different median filter masks (windows) designed for the sub-bands. The masks for the vertical and horizontal direction are applied as any median filter mask is applied. The masks for diagonal direction are designed for 45 degrees and 135 degrees.

The method to determine the diagonal direction to be used is:

a. The absolute values of coefficients are sorted from low to high in both the directions (45 degrees and 135 degrees).
b. The difference of sorted coefficient is calculated by the equations below (refer to Figure 3.11 below):

$$d_1 = \big||A(i-1,j-1)| - |A(i+1,j+1)|\big|$$

$$d_2 = \big||A(i-1, j+1)| - |A(i+1, j-1)|\big|$$

Where *A(i,j)* is the selected pixel. If $d_1 >= d_2$, the window of 135 degrees is selected to process the coefficient, else the window of 45 degrees is selected to process the coefficient. An example is shown below in Figure 3.12.

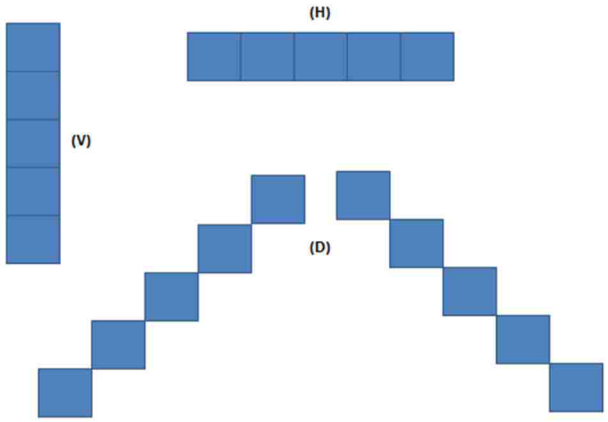

Figure 3.10 Shapes of DAMF [22]

A(i-2,j-2)				A(i-2,j+2)
	A(i-1,j-1)		A(i-1,j+1)	
		A(i,j)		
	A(i+1,j-1)		A(i+1,j+1)	
A(i+2,j-2)				A(i+2,j+2)

Figure 3.11 Diagonal directional filter of DAMF

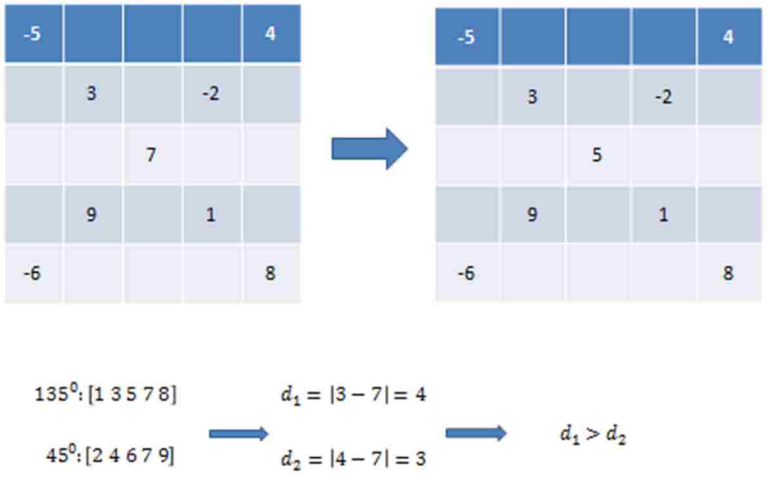

Figure 3.12 Example of diagonal directional filter of DAMF

3.5.3 Results. Figure 3.13 below shows the de-noising technique applied to a mammogram.

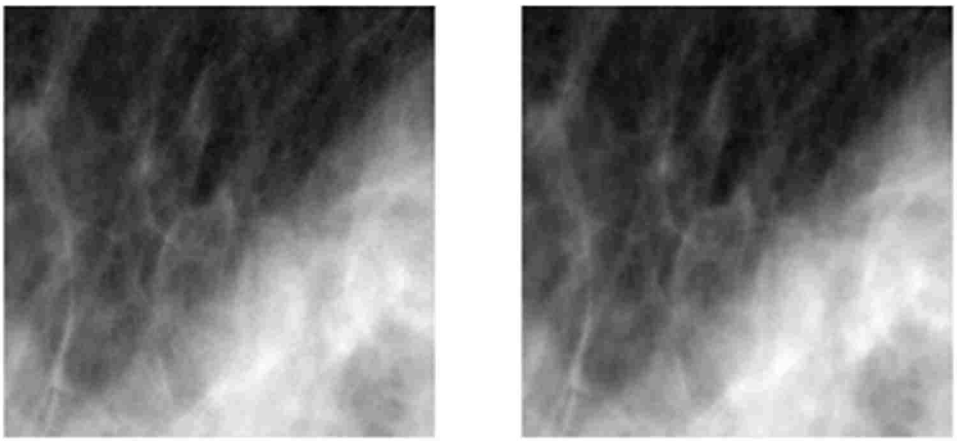

Figure 3.13 Original mammogram (512 x 512) (left); mammogram de-noised by IBS and DAMF (right)

3.5.4 Discussion and Analysis. The image on the left in Figure 3.13 is de-noised using the technique discussed. A significant reduction in noise can be noted visually. As discussed earlier, the technique is applied to the Lena image with added Gaussian and Poisson noise to quantify the performance of the technique. Figure 3.14 below shows the results.

Figure 3.14 IBS and DAMF - Lena image with Gaussian noise (top-left); de-noised version of Lena image with Gaussian noise (top-right); Lena image with Poisson noise (bottom-left); de-noised version of Lena image with Poisson noise (bottom-right)

As evident from Table 3.5 below, there is a significant improvement in PSNR by using the IBS and DAMF filter. At a decomposition level of 5, the technique applied to Lena image with Gaussian noise yields a PSNR of 28.5196 dB which is close to 9dB higher than the noisy image. Similar results are obtained even on the Lena image with Poisson noise. As expected, the PSNR increases with increasing decomposition levels. It saturates at a decomposition level of 5.

Table 3.5 Comparing PSNR by applying IBS and DAMF at different decomposition levels

	Lena with Gaussian(dB)	Difference in PSNR	Lena with Poisson(dB)	Difference in PSNR
Noisy	19.7159	0	26.8444	0
Level 1	24.6437	4.9278	30.1571	3.3127
Level 2	27.8683	8.1524	31.7713	4.9629
Level 3	28.2165	8.5006	32.0939	5.2495
Level 4	28.5083	8.7924	32.3194	5.475
Level 5	28.5196	8.8037	32.6862	5.8418

4. CONCLUSION

The five techniques presented treat the wavelet coefficients in different manners to find a threshold for wavelet shrinkage. The results obtained are presented together here in Tables 4.1 and 4.2:

Table 4.1 Comparison of all techniques on Lena image with added Gaussian noise w.r.t. difference in PSNR (in dB)

	Daubechies Complex wavelet	Adaptive feature-based	Noise deviation estimation	BayesShrink	Modified BayesShrink +DAMF
Level 1	4.9638	4.3652	5.0139	5.0185	4.9278
Level 2	**5.7497**	6.7268	**6.8044**	7.3193	8.1524
Level 3	3.4839	**7.5112**	6.4902	7.743	8.5006
Level 4	0.9072	7.0072	6.0623	7.7794	8.7924
Level 5	-1.115	4.4169	5.8606	**7.7822**	**8.8037**

In Tables 4.1 and 4.2 above, the highest obtained values of difference (between noisy and de-noised images) in PSNR values are bolded. It can be inferred that the BayesShrink approach and the Modified BayesShrink approach with DAMF produce the best results. As seen from the Tables 4.1 and 4.2 above, the PSNR's of the noisy images are differ slightly with an average deviation of about 0.015dB. This happens because the noise is added using MATLAB. The noise addition algorithm used by MATLAB adds noise randomly to the image each time it is used.

Hence, there is a slight difference in the noisy images produced which accounts for the slight difference in PSNR's.

Table 4.2 Comparison of all techniques on Lena image with added Poisson noise w.r.t. difference in PSNR (in dB)

	Daubechies Complex wavelet	Adaptive feature-based	Noise deviation estimation	BayesShrink	Modified BayesShrink +DAMF
Level 1	**2.1607**	1.8768	**2.9343**	3.4401	3.3127
Level 2	-0.4552	2.3319	2.7283	4.2512	4.9629
Level 3	-3.5151	**3.9517**	2.1634	4.3385	5.2495
Level 4	-6.203	1.839	1.8737	4.3435	5.475
Level 5	-8.2415	1.1393	1.771	**4.3487**	**5.8418**

It can also be seen that the highest PSNR values are obtained at higher decomposition levels. This means that, the more an approach can penetrate into higher decomposition levels without harming the edges, the better the performance it will have.

This thesis presents a study of leading noise reduction techniques in mammograms based on the wavelet domain. The next step after noise reduction is to enhance contrast. These de-noised images should be enhanced in contrast and evaluated by radiologists. The feedback received from radiologists and the results obtained from the study presented should be used to develop certain adaptive techniques for noise-reduction which would improve the visual quality of mammograms and serve as a better aid in early detection of breast cancer.

BIBLIOGRAPHY

[1] Loza A., David Bull, Alin Achim, "Automatic Contrast Enhancement of Low-Light Images Based on Local Statistics of Wavelet Coefficients," IEEE 17th International Conference on Image Processing, 2010, 3553-3556

[2] Mahesh Mahadevappa, "Digital Mammography: An Overview," RadioGraphics, RSNA 2004, Vol 24, No. 6, p 1747-1760

[3] *Image Noise*. Retrieved June 30, 2011, from http://www.sprawls.org/ppmi2/NOISE/

[4] *Poisson distribution*. Retrieved November 25, 2011, from http://en.wikipedia.org/wiki/Poisson_distribution

[5] N Oberhofer, G Compagnone, E Moroder, "Use of CNR as a metric for optimisation in digital radiology," Proceedings - World Congress on Medical Physics and Biomedical Engineering: Diagnostic Imaging, v 25 IFMBE, n 2, p 296-299, 2009

[6] Alain Hore, Djemel Ziou, "Image quality metrics: PSNR vs. SSIM," Proceedings - International Conference on Pattern Recognition, p 2366-2369, 2010

[7] Rafael C Gonzalez, Richard E. Woods, "Digital Image Processing," Third Edition. New Jersey: Pearson Prentice Hall, 2008

[8] Stefan Schulte , Bruno Huysmans, Aleksandra Pi˘zurica, Etienne E. Kerre1, Wilfried Philips, "A New Fuzzy-Based Wavelet Shrinkage Image Denoising Technique," ACIVS 2006, LNCS 4179, pp. 12–23, 2006

[9] Laine A., Jian Fan and Wuhai Yong, "Adaptive Multiscale Processing for Contrast Enhancement," SPIE, 1993, Vol 1905/521, 521-53

[10] Heinlein Peter, Johann Drexl, and Wilfried Schneider, "Integrated Wavelets for Enhancement of Microcalcifications in Digital Mammography," IEEE Transactions On Medical Imaging, 2003, Vol. 22, No. 3, 402-413

[11] Du Shan, Ward Rabab, "Wavelet-Based Illumination Normalization For Face Recognition," IEEE 0-78003-9134-9/05, 2005

[12] Zhen-Bing Zhao, Jin-Sha Yuan, Qiang Gao, Ying-Hui Kong, "Wavelet image de-noising method based on noise standard deviation estimation," Proceedings of the International Conference on Wavelet Analysis and Pattern Recognition, NOV. 2007

[13] D. L. Donoho, "De-noising by soft-thresholding," IEEE Trans. Inform. Theory, vol. 41, pp. 613–627, May 1995.

[14] D. L. Donoho and I. M. Johnstone, "Ideal spatial adaptation via wavelet shrinkage," Biometrika, vol. 81, pp. 425–455, 1994.

[15] I. Daubechies, Ten Lectures on Wavelets (SIAM, 1992)

[16] Moongu Jeon, Uma Shanker Tiwary, Ashish Khare, "Daubechies complex wavelet transform based multilevel shrinkage for deblurring of medical images in presence of noise," International Journal of Wavelets, Multiresolution and Information Processing, Vol. 7, No. 5 (2009) 587–604

[17] Karunesh K. Gupta, Rajiv Gupta, "Feature Adaptive Wavelet Shrinkage for Image Denoising," IEEE – ICSCN, p 81-85, 2007

[18] S. Grace Chang, Bin Yu, Martin Vetterli, "Adaptive Wavelet Thresholding for Image Denoising and Compression," IEEE transactions on Image Processing, Vol. 9, No. 9, SEP. 2000

[19] J. Immerker, "Fast noise variance estimation," Computer Vision and Image Understanding, Vol.64, No.2, pp.300-302, 1996

[20] Zhen-Bing Zhao, Jin-Sha Yuan, Qiang Gao, Ying-Hui Kong, "Wavelet image de-noising method based on noise standard deviation estimation," Proceedings of the International Conference on Wavelet Analysis and Pattern Recognition, NOV. 2007

[21] David L. Donoho, Iain M. Johnstone "Adapting to unknown smoothness via wavelet shrinkage," Journal of the American Statistical Assoc., vol. 90, no. 432, p 1200–1224, December 1995.

[22] Ling Wang, Jianming Li, Yegiu Li, Takashi Yahagi, Takahide Okamoto, "Noise Reduction Using Wavelet with Application to Medical X-ray Image," Proceedings of the IEEE International Conference on Industrial Technology, p 33-38, 2005

VITA

Varun Shah was born in Hyderabad, India. He received his Bachelor of Technology degree in Electronics and Instrumentation Engineering from Vellore Institute of Technology, Vellore, India. He joined Missouri University of Science and Technology in Fall 2010 to pursue his Master of Science degree in Electrical Engineering.

Varun held a Graduate Research Assistantship with Dr. Hyoung Koo Lee where he worked on enhancement of radiography images. His other interests include Digital Design, Mixed-signal Design and Digital Logic. He received his M.S in Electrical Engineering in December 2012.